Optical and Quantum Electronics (2023) 55:85
https://doi.org/10.1007/s11082-022-04371-7

Computational study of non-linear optical and electrical properties of 1,3-dinitropyrene

Shradha Lakhera[1] · Meenakshi Rana[1] · Kamal Devlal[1] · Vivek Dhuliya[2]

Received: 17 August 2022 / Accepted: 5 November 2022 / Published online: 12 December 2022

Abstract

This study aims to explore the optoelectronic properties of a pyrene derivative 1,3-dinitropyrene using density functional theory to determine molecular electrostatic potential and Van der Waals surface, frontier molecular orbitals, and molecular orbital surfaces. The Mulliken charges, molecular electrostatic potential, and Van der Waals surface are accounted to show the availability of the electron donor-acceptor moieties, resulting in the charge transfer within the molecule. Theoretical electronic spectra are computed using Time-dependent density functional theory that shows the charge transfer process between nitro groups and C–H bonds of benzene rings. Vibrational features and chemical shifts are evaluated using Raman spectra and nuclear magnetic resonance shifts. The computed first-order hyperpolarizability of 1,3-dinitropyrene is 26 times higher than that of Urea showing its immensely high non-linear optically active responses. The smaller reorganization energy for hole transportation of the 1,3-dinitropyrene validates its application as a hole transport layer in organic light-emitting diodes.

Keywords 1,3-dinitropyrene · Density functional theory · Nonlinear optical material · Reorganization energy · Organic light emitting diode

Abbreviations

CP	Chemical potential
DFT	Density functional theory
DSSC	Dye synthesized solar cell
DNP	1,3-dinitropyrene
EA	Electron affinity
FMO	Frontier molecular orbital
HOMO	Highest occupied molecular orbital
ICT	Intramolecular charge transfer
IP	Ionization potential

✉ Meenakshi Rana
mrana@uou.ac.in

[1] Department of Physics, School of Sciences, Uttarakhand Open University, Haldwani, Uttarakhand 263139, India

[2] Department of Physics, Gurukula Kangri (Deemed to be University), Haridwar, Uttarakhand 249404, India

LHE	Light harvesting efficiency
LUMO	Lowest unoccupied molecular orbital
MEP	Molecular electrostatic potential
NLO	Nonlinear optics
NMR	Nuclear magnetic resonance
OLED	Organic light emitting diode
RE	Reorganization energy
SPE	Single point energy
TD-DFT	Time dependent density functional theory

1 Introduction

In the past thirty years, the research industry has given a hike to nonlinear optical (NLO) materials and their applications. Extensive research has been carried out on organic, semi-organic, or inorganic, kind of materials so far. Organic NLO compounds, although, have many advantages over the other kind due to their enhanced efficiency, larger molecular polarizability, and rapid response times (Abusaif et al. 2021; Lakhera et al. 2022; Ozarslan et al. 2020). The availability of π-based electronic delocalization results in rapid responsiveness in organic materials that leads to high NLO activity of materials (Buriahi et al. 2020). The outspread applications of NLO materials in photonics, telecommunications, frequency mixing, optical computing, electro-optical devices, molecular switches, dynamic holography, lasers, luminescent materials, microfabrication, data storage, spectroscopic and electrochemical sensors, etc., have made them an attractive and contemplating corner of research (Mary et al. 2019; Ray and Ray 2010). Therefore, different classes of excellent NLO materials have been studied. It is reported that the organic compounds containing electron-donating aromatic part and electron-accepting nitro group show tremendous intramolecular interactions leading to the enhancement of NLO activity (Lakhera et al. 2021). The occurrence of intramolecular charge transfer (ICT) accounts for the high reactivity of the molecule that is considered the base in predicting the optical nonlinearity of the materials (Abusaif et al. 2021). One such category of organic molecules consisting of π-donor and acceptor moieties is Pyrene and its derivatives. Pyrene derivatives are polycyclic aromatic hydrocarbons having planar aromatic geometries consisting of clubbed benzene rings. The incomplete combustion of organic compounds gives rise to pyrene and its derivatives (Wazzan et al. 2018). Pyrene and its derivatives are known to have wide applications as dyes in solar cells applications. Compounds like Phenothiazine conjugated ethynyl-pyrene (Nagarajan et al. 2017), conjugated pyrene-cored perylene diimide (Tang et al. 2019), N-octakis(4-methoxyphenyl) pyrene-1,3,6,8-tetraamine (Andijani et al. 2019)are known for their proven uses as dyes for solar cells. Many studies report the NLO activity of the pyrene derivatives hydroxypyrene (Felscia et al. 2018), methyl (E)-2-cyano-3-(5-(pyren-1-yl) thiophen-2-yl)-3-acrylate (Khalid et al. 2021), pyrene-core arylamine derivatives (Andijani et al. 2018), enzoyl acetone pyrene (More et al. 2017)etc., are available which shows high chemical reactivity of pyrene. Some studies on Pyrene-containing chalcone derivatives (Sun et al. 2019), 1-(pyren-1-yl) − 3-(4-Methyl thiophene-2-yl) acrylic ketone and 1-(pyren-1-yl) − 3-(4-bromo thiophene-2-yl) acrylic ketone (Shi et al. 2017), (E)-3-(6-(methoxypyridin-3-y1)-1-(pyren-1-yl) prop-2-en-1-one) and (E)-3-(2, 6-dichlorophenyl)-1-(pyren-1-yl) prop-2-en-1- one (Niu et al. 2018) reporting the properties of pyrene derivatives in third-order nonlinearity have also been observed. Wide applications of pyrene

derivatives have been reported which shows the high chemical reactivity of the pyrene. Thus, motivated by this fact, one such pyrene derivative 1,3-dinitropyrene (DNP) having planar aromatic two-dimensional geometry has been considered for the present study.

The main objective of the presented work is to discover enhanced polarizability and hyperpolarizability of DNP molecule that relates to charge transport within the molecule. Thus, the charge transferring parts will be identified in the study using Mulliken charge distribution and global reactivity parameters. The location of electrophilic and nucleophilic parts of DNP are identified by molecular electrostatic potential (MEP) and Van der Waals surface. The spectral features of DNP are also presented by using computed Raman, UV-Vis, and Nuclear magnetic resonance (NMR) spectra. The hyperpolarizability parameters and cationic and anionic energies are analyzed for developing the NLO activity of the molecule and its application in organic light-emitting diodes (OLED) respectively.

2 Computational procedure and calculation

The structure of the DNP is downloaded from the online database "PubChem" (https://pubchem.ncbi.nlm.nih.gov/) in sdf format and converted into gjf format using software "OpenBabel" (http://openbabel.org/wiki/Main_Page). Density functional theory (DFT) method is used for all the quantum chemical calculations using Gaussian 09 packages (M.J. 2009). The interpretation of the output is done using GUI Gauss View 5.0 (R. 2007). Becke-3-Lee-Yang-Parr (B3) exchange function combined with (LYP) correlation is used for ground state geometry optimization of DNP molecule. Standard B3LYP/6-311G basis set is used for all ground states as well as cationic and anionic optimizations (Becke and Becke 1993; Becke and Becke 1997). The ground state optimization were carried out till threshold values of maximum force as 0.00045, RMS force 0.0003, maximum displacement 0.0018 and RMS displacement 0.0012 without any additional information sets. Minimization of the molecule's geometry downloaded from PubChem database was without any constraint leading to true minima. The optimization of the molecule was carried out in gas phase at T = 298.15 K and 1 atmosphere pressure without fixing any parameter or coordinate. The free energy is computed for DNP molecule by the following given expression:

$$E_{free} = E_{electronic} + E_{thermal}$$

where $E_{electronic}$ and $E_{thermal}$ are the electronic and thermal energy respectively. Different reactivity parameters like bandgap (ΔE), ionization potential (IP), electron affinity (EA), chemical potential (CP), electronegativity (χ), softness (S), and hardness (η) are calculated with the help of Koopman's equations given below (Koopmans and Koopmans 1933):

$$\Delta E = E_{LUMO} - E_{HOMO} \tag{1}$$

$$IP = -E_{HOMO} \tag{2}$$

$$EA = -E_{LUMO} \tag{3}$$

$$CP = \frac{E_{HOMO} + E_{LUMO}}{2} \tag{4}$$

$$\chi = \frac{(IP + EA)}{2}, \tag{5}$$

$$\eta = \frac{E_{LUMO} - E_{HOMO}}{2}, S = \frac{1}{\eta}, \tag{6}$$

The Van der Waals surface is computed using software "Avogadro" (https://avogadro.cc/) (Yadav et al. 2021). The electronic spectra is computed using time-dependent density functional theory (TD-DFT) for self-consistent field (SCF) approach for nine transitions. For TD-SCF calculations, convergence on RMS density matrix was at 1.00×10^{-8}, convergence on maximum density matrix was at 1.00×10^{-6}.

The vibrations of different bonds of DNP molecule are studied using computed vibrational spectra. The reactivity and high polarizability of the DNP molecule is developed by computing Raman intensity using the given expression (Rana et al. 2017; Felscia et al. 2018):

$$I = \frac{f\left(\nu_o - \nu_i\right)^4 \mathrm{S}_i}{\nu_i\left[1 - \exp\left(-\frac{hc\nu_i}{\mathrm{kT}}\right)\right]} \tag{7}$$

where I refers to Raman intensity of the considered mode, f is a constant with value 10^{-12}, ν_o has value 9398.5 cm^{-1}. ν_i and S_i are the vibrational wavenumber and Raman activity of selected mode respectively. h is Planck constant with value 4.1357×10^{-15} eV K^{-1}, c is speed of light having value 3×10^8 m/s, K is Boltzmann constant with value 8.6173×10^{-5} eV K^{-1}, and T is temperature 293.5 K. NMR analysis was also done using Gauge-Independent Atomic Orbital method including nuclear spin. Tetramethylsilane (TMS) at 298.15 K temperature and 1 bar pressure was taken as the internal reference compound. Polarizability parameters are calculated to understand the diffusion of the electron cloud in compound and are used for developing the NLO behavior of the title molecule. The polar frequency calculations are performed for obtaining the tensor components of total dipole moment (μ_{total}), total isotropic polarizability (α_{total}), anisotropy of polarizability ($\Delta\alpha$) and first order hyperpolarizability (β_{total}) using finite field theory approach. These parameters are computed using below given expression:

$$\mu_{total} = \left(\mu_x^2 + \mu_y^2 + \mu_z^2\right)^{\frac{1}{2}} \tag{8}$$

$$\alpha_{total} = \frac{1}{2}\left(\alpha_{xx} + \alpha_{yy} + \alpha_{zz}\right) \tag{9}$$

$$\Delta\alpha = \frac{1}{\sqrt{2}}\left[\left(\alpha_{xx} - \alpha_{yy}\right)^2 + \left(\alpha_{yy} - \alpha_{zz}\right)^2 + \left(\alpha_{zz} - \alpha_{xx}\right)^2 + 6\alpha_{xz}^2 + 6\alpha_{xy}^2 + 6\alpha_{yz}^2\right]^{\frac{1}{2}} \tag{10}$$

$$\beta_{total} = \left[\left(\beta_{xxx} + \beta_{xyy} + \beta_{xzz}\right)^2 + \left(\beta_{yyy} + \beta_{yzz} + \beta_{yxx}\right)^2 + \left(\beta_{zzz} + \beta_{zxx} + \beta_{zyy}\right)^2\right]^{\frac{1}{2}} \tag{11}$$

where μ_x, μ_y, and μ_z are the tensor components dipole moment, α_{xx}, α_{yy}, and, α_{zz} are the tensor components of polarizability and β_{xxx}, β_{yyy}, and β_{zzz} are the tensor components of hyperpolarizability.

In order to define the application of title molecule in OLED, Reorganization energy (RE) is computed for the DNP. The RE is a measure of charge transport capability of the molecular systems and is computed using single point energies (SPE) by following given equations (Si et al. 2011):

$$\lambda_i = \lambda_e + \lambda_h \tag{12}$$

$$\lambda_e = \left(E_0^- - E_-^-\right) + \left(E_-^0 - E_0^0\right) \tag{13}$$

$$\lambda_h = \left(E_0^+ - E_+^+\right) + \left(E_+^0 - E_0^0\right) \tag{14}$$

where, E_0^0= SPE of ground state geometry, E_0^-= SPE of anion state optimization of ground state geometry, E_-^- = SPE of anion state optimization of anion molecule, E_-^0 = SPE of ground state optimization of anion state geometry, E_0^+= SPE of cation state optimization of ground state geometry, E_+^+= SPE of cation state optimization of cation state and E_+^0= SPE of ground state optimization of cation state geometry of the molecule.

Light harvesting efficiency (LHE) is also computed for the DNP using the oscillator strength (*f*) by using the below mentioned formula (Curutchet et al. 2017; Sang-aroon et al. 2019):

$$LHE = 1 - 10^{-f} \tag{15}$$

LHE is the measures of applicability of the molecule to be used as photosensitizers in Dye Sensitizer Solar Cells (DSSC) (Lakhera et al. 2022; Abusaif et al. 2021). The organic molecules are reported to have high LHE. Thus, these materials are in great demand for enhancing the efficiency of solar cells.

3 Results and discussion

3.1 Structure analysis

Figure 1 illustrates the optimized geometry of DNP. The benzene rings are settled in planar geometry with C1 point group symmetry. The non-planarity is observed by the deviation in the 1O–5N–3O and 2O–6N–4O bonds of the nitro groups. The molecule comprises four inter-connected benzene rings with two nitro groups 1O–5N–3O and 2O–6N–4O bonded with the benzene. The electrostatic potential energy is computed as -27892.29 eV. The computed value of free energy of the DNP molecule is -642864.55 kcal/mol. Molecules with high intramolecular interactions are known to have high polarizability. The higher value of dipole moment of 9.07 Debye is computed for the DNP molecule which shows the high polarity of the molecule. The optimal parameters like bond lengths and bond angles are also analyzed for DNP. The low value of bond length shows the higher stability of the molecules. Although, the bond angles are inversely proportional to the bond lengths. The optimized bond lengths and angles of the DNP are listed in SD 1 and SD 2 respectively. The bonds 17C–25H, 20C–28H, 22C–30H, 21C–29H, and 18C–26H are the outer C–H bonds of the benzene rings. These bonds have same bond length equal to 1.08 Å. The bonds 2O = 6N, 4O = 6N, 3O = 5N, and 1O = 5N are associated with the nitro groups. These bonds have a comparatively higher bond length equal to 1.22 Å. The bond angles between nitro groups were observed at around 122.74°. This was found to be higher than

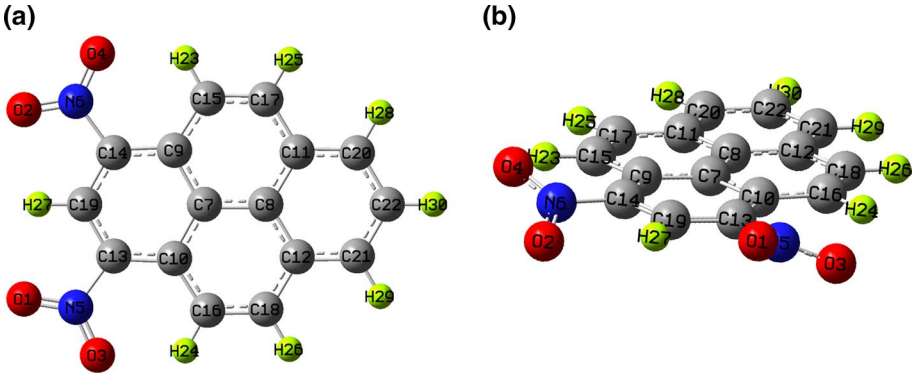

Fig. 1 (**a**) Front view of optimized structure of DNP, (**b**) Side view of the geometry showing the non-planar arrangement of the nitro group and planar geometry of benzene rings in DNP molecule

bond angles corresponding to C–H bonds of the benzene rings. Thus, the optimal parameters highlighted the nitro groups and the C–H bond of benzene rings are the most reactive regions of the molecule.

3.2 Charge analysis

Charge analysis is done to investigate the location where the charge is transferred and the moieties that are participating in the transferring of the charge. Molecules possessing immense ICT are considered chemically reactive (Rana et al. 2016). In DNP, the computed Mulliken charges accounted for the positive charge contribution of the hydrogen atoms and the negative charge contribution of 5 and 6N atoms. The Mulliken charge distribution in the DNP molecule is plotted in Fig.2. The carbon atoms, however, contributed positively as well as negatively charges. The nitrogen atoms of nitro groups have a negative charge equal to −0.214 and − 0.214 e. The 1O, 2O, 3O and 4O oxygen atoms have charges equal to 0.033, 0.033, 0.009 and 0.009e respectively. The hydrogen atoms 23H, 25H, 28H, 30H, 29H, 26H, and 24H corresponding to the outer C–H atoms of the benzene rings have positive charges and the carbon atoms of these C–H atoms like 15C, 17C, 20C, 22C, 21C, 18C, and 16C have the negative charge magnitudes. Thus, there found a major charge variation between the nitro groups and the C–H bonds of the benzene rings. This charge variation might be considered due to the occurrence of intramolecular interactions in the DNP molecule. Thus, the Mulliken charge analysis suggests the existence of intramolecular interactions between the nitro groups and C–H bonds.

3.3 Chemical reactivity analysis

The global reactivity parameters are computed for DNP using Koopman's equations. These parameters are called frontier molecular orbitals as they deal with the highest occupied and lowest unoccupied molecular orbitals (HOMO and LUMO). These orbitals are of frontier electron occupation and have a large influence on the chemical properties. The energy corresponding to these frontier HOMO and LUMO were − 6.82 and − 3.66 eV respectively. The difference between these energies is denoted as ΔE and its value of 3.16 eV. The lower

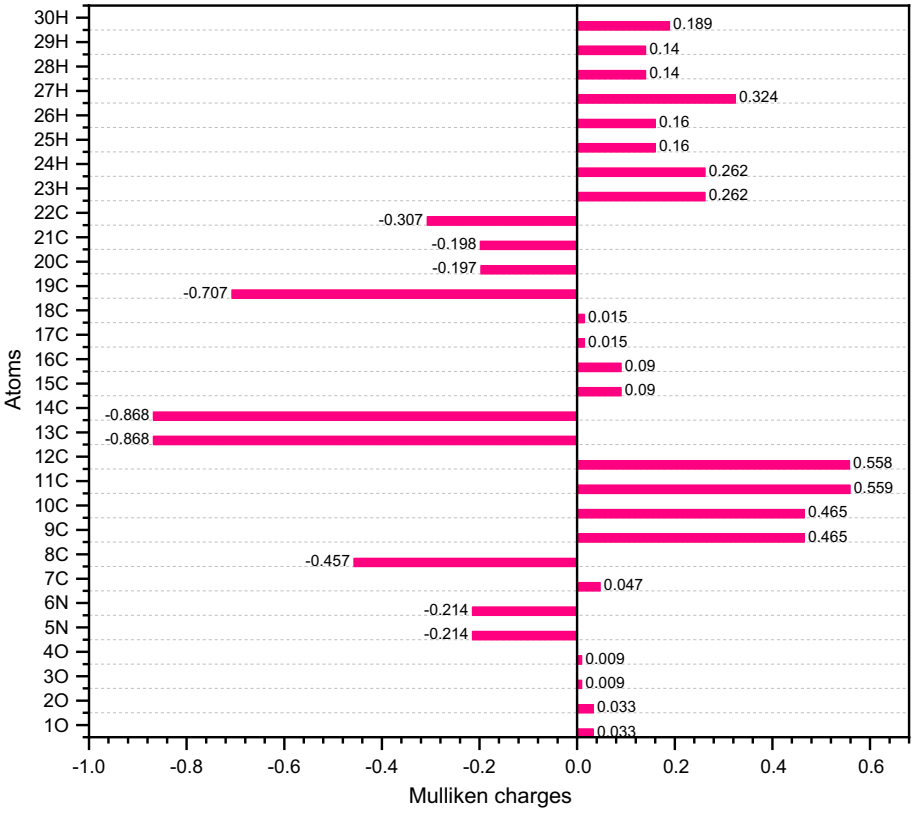

Fig. 2 Mulliken charge plot for optimized DNP molecule

value of ΔE shows that the electrons in the HOMO can easily jump up to the LUMO and can leads to the occurrence of electronic transitions easily (Bhatt et al. 2020). The ΔE for the generally used reference materials Urea is 7.43 eV and the ΔE for DNP is much lower than the ΔE of Urea. The other computed global reactivity parameters are mentioned in SD 3. The value of *IP* for DNP is calculated as 6.82 eV which is high enough to show the easy drifting tendency of electrons in the outermost orbitals of the atom. These electrons become free electron pairs for bond formation. The *EA* (3.66 eV) shows the tendency of the molecule to accept the free electron pairs and form a bond with the donating atom. The value of *CP* is computed as −5.24 eV indicating the energy associated with the overall process of sharing electrons. The high value of χ (5.24 eV) shows the high ability of atoms to attract the free electrons for bond formation. The value of η for DNP is calculated as 1.58 eV. This shows that the DNP molecule has good chemical hardness. On the contrary, the value of S for DNP is 0.63 eV which is lower than the η indicating the rigidness and stiffness of the DNP molecule. Figure 3illustrated the distribution of HOMO-LUMO surfaces over the geometry of the probe molecule. The positive and negative phases in molecular orbital wave function are represented by red and green color surfaces respectively (Jeyaram et al. 2020). The 17C and 21C show the transformation from red color in HOMO to green color surface in LUMO respectively. This indicates the transformation of these atoms from positive to negative charge. The atoms 18 and 20C show the transformation from green to red

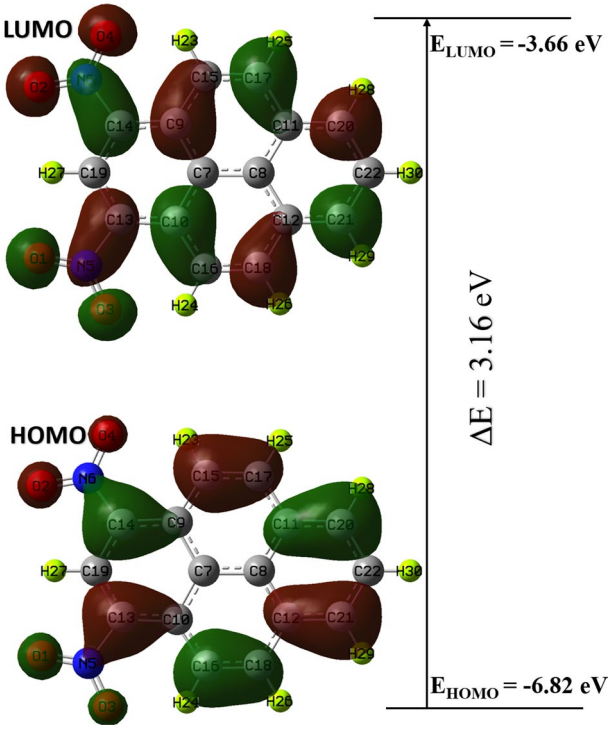

Fig. 3 HOMO and LUMO with respective energies illustrating the energy difference between these orbitals

indicating the change from negative to positive. The rest of the HOMO-LUMO distribution remains unchanged. This indicates that 17C, 18C, 20C, and 21C majorly lead to transferring of the charge cloud within the DNP molecule. Thus, all the above-given data validates that the DNP molecule undergo immense ICT.

3.4 Molecular electrostatic potential and Van der Waal surface analysis

Figure 4a illustrates the MEP surface of DNP. The MEP surface facilitates the identification of the negative, positive, and zero potential regions of the molecule (Lakhera et al. 2022). The red, blue, and green colored regions of the MEP surface indicate the electrophilic, nucleophilic, and neutral regions of the molecule respectively. The magnitude of electrostatic potential is in order of blue > green > yellow > orange > red, i.e., the blue color is the region with high electrostatic potential and thus acts as a charge donating region, whereas the red color has the low electrostatic potential and acts as accepting regions (Sethi et al. 2015). In MEP of DNP, the blue color spread over the C–H bonds of the benzene rings. This shows that the bonds 17C–25H, 20C–28H, 22C–30H, 21C–29H, and 18C–26H act as the nucleophilic part within the DNP molecule. On the other hand, the nitro groups 2O = 6N = 4O and 3O = 5N = 1O have a red color surface over them indicating their electrophilic nature. Thus, the MEP surface shows that both the nitro groups are responsible for the generation of the free charge cloud and the charge cloud seemed to be transferred from nitro groups to the C–H bonds of the benzene rings. The magnitude of the positive and negative electrostatic potential of DNP is shown as a color bar at the top of the MEP surface. The range of electrostatic potential of the DNP molecule is computed as

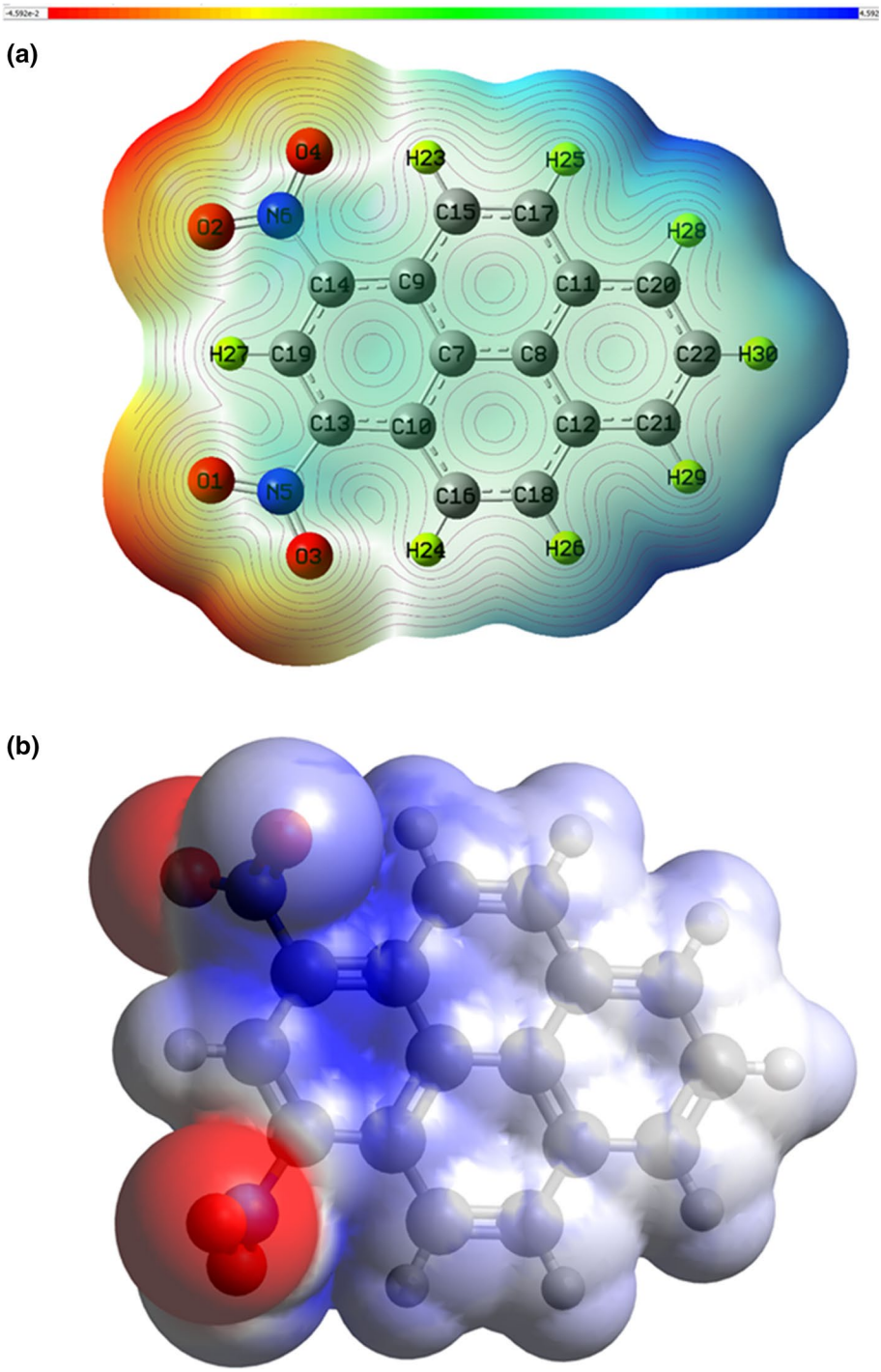

Fig. 4 (**a**) Molecular electrostatic potential surface of DNP illustrating electrophilic region in blue and nucleophilic region in red colour, (**b**) Van der Waal surface of DNP illustrating electropositive region as blue and electronegative region as red surface

$\pm 4.59 \times 10^{-2}$ electrons/Å^3. The contour lines are also shown on the MEP surface. These lines indicate the higher magnitude of the electrostatic field in the region, where the lines are largely accumulated (Ojo et al. 2020). Thus, the dense collection of the contour lines near the nitro groups and the outer C–H bonds of the benzene rings indicates that these bonds will experience more field and will be majorly altered by the field. This alteration will lead to the weakening of these bonds and there are great chances of these bonds getting dissociated. Hence, the presence of the contour lines near nitro groups and C–H bonds indicates that the intramolecular interactions will most probably occur between nitro groups and outer C–H bonds of the benzene rings.

The Van der Waals surface is shown in Fig. 4b. The Van der Waals surface reveals the intramolecular interactions. The blue and red-colored regions indicate the electropositive and electronegative regions of the molecule respectively (John et al. 2020). The Van der Waals surface of DNP reveals that the nitro groups act as high electronegative parts and the benzene rings act as electropositive parts. Thus, the MEP and Van der Waals surface, both validate the existence of intramolecular interactions of the DNP molecule within the nitro groups and C–H bonds of the benzene rings.

3.5 Vibrational analysis

A complete vibrational mode analysis has been done for all the Raman modes obtained from the computed vibrational spectra. The vibrational Raman modes account for the NLO activity of any compound as the Raman intensity is proportional to the polarizability of the compound (Lakhera et al. 2022). A few of the major Raman modes are shown in Fig. 5. Different modes observed for different bonds in DNP molecules are listed in SD 4. The bonds 13C–5N and 14C–6N connecting the nitro groups to the benzene rings show linear symmetric stretching (ν_{CN}) at frequency 334.35 cm^{-1} and twisting ($\tau_{14C-6\ N}$) at 665.98 cm^{-1}. The nitro groups, however, show a peak for torsional bending (δ_{ON}) of bonds 3O–5N and 4O–6N at a frequency of 367.83 cm^{-1}. Multiple vibrations due to the bending of C–C bonds of the benzene rings (θ_{CC}) are observed in the frequency range 313-554.44 cm^{-1}. At 523.16 cm^{-1}, the bonds12C–21C and 12C–22C of the benzene show wagging (ω_{CC}). The modes due to the wagging of C–H bonds (Ω_{CH}) are observed in the range 873.46–894.3 cm^{-1}. The torsional bending of bonds 13C–5N and 14C–6N (δ_{CN}) gave a sharp peak at 897.18 cm^{-1}. The δ_{CH} for 21C–29H and 20C–28H showed a peak at 1136.67 cm^{-1}. The other δ_{CH} modes are observed between 1214.43 and 15309.18 cm^{-1}. The rocking of C–H bonds (ρ_{CH}) is observed at 1480.11, 1533.95, and 1558.95 cm^{-1}. The ν_{CC} modes were observed between 1580.72 and 1677.4 cm^{-1}. A high peak is observed for ν_{CC} mode at 1677.4 cm^{-1}. The asymmetric linear stretching of the nitro group (α_{ONO}) has a sharp peak at 1710.68 cm^{-1}. The α_{CH} modes were observed between 1718.76 and 3158.35 cm^{-1}. The mode with the highest frequency was ν_{CH} for 16C–24H and 15C–23H at 3261.84 cm^{-1}. The Raman modes obtained for the DNP molecule reveal that high Raman intensity of the vibrating modes are obtained for the vibrations associated with nitro groups and C–H bonds. The high Raman intensity is proportionally related to the polarizability of the molecule. Thus, the high Raman intensity obtained for the active region modes of the DNP molecule imparts to the occurrence of high polarizability of the molecule.

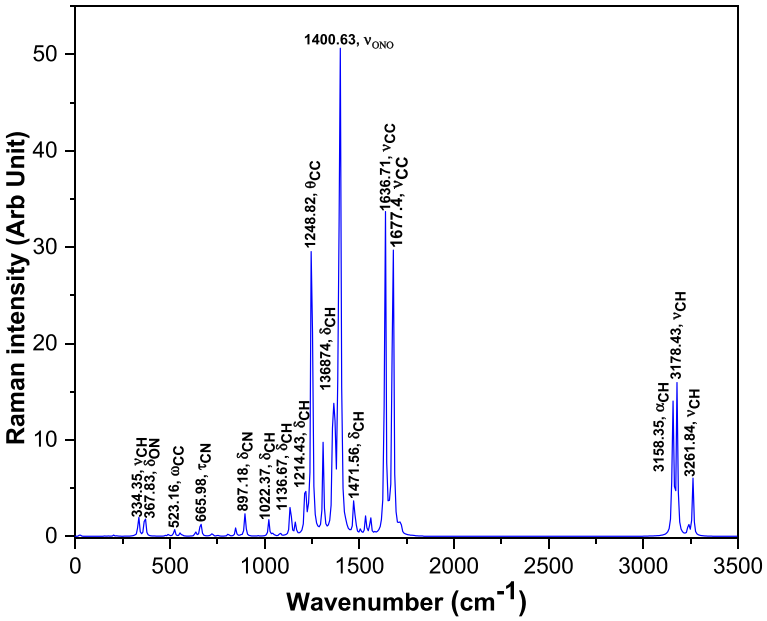

Fig. 5 Computed Raman spectra of DNP showing different vibration modes (Symmetric stretching-ν, asymmetric stretching-α, torsional bending in plane (scissoring)-δ, twisting-τ, rocking-ρ, and wagging-ω, bending of C–C bonds in benzene- θ, stretching of C–C bonds in benzene- λ)

3.6 Absorption spectral analysis

The computed absorption spectra (Fig. 6) have been shown for the first nine transitions to account the electronic transitions of the DNP molecule. Two absorption bands were obtained for DNP molecule between 200–325 and 330–475 nm. The details of the transitions were listed in SD 5. For the better validation, the experimental details of the absorption spectra of DNP are considered from the study of M. B. Brister (Brister et al. 2017). Two major experimental absorption bands of the DNP were observed between 250–310 and 350–460 nm wavelength (Brister et al. 2017) which is in good agreement with the simulated spectral range. The $S_0 \rightarrow S_1$ transition of the simulated absorption spectra occurring at 373 nm wavelength was mainly responsible for the absorption band between 330–475 nm range having value of oscillator strength (*f*) of 0.4917 and excitation energy of 3.31 eV. The experimental peak of the absorption band between 350–460 nm ranges is approximately around 440 nm that is indicated in the inset of Fig. 6. The transitions from $S_0 \rightarrow S_5$ to $S_0 \rightarrow S_9$ of the simulated absorption spectra lies in band 200–325 nm. However, the $S_0 \rightarrow S_6$transition has the maximum oscillator strength of 0.225 and thus majorly contribute in the formation of the absorption band between 200–325 nm giving a peak at 286 nm. Parallelly, the peak of experimental absorption spectra lies approximately at 280 nm in 250–310 nm range (Brister et al. 2017; Chen et al. 2021). The spectral range of computed absorption and the experimental absorption in the mentioned references was close enough to validate the computational calculations. However, this slight difference might be due to the fact that computational spectra deal with the single molecule simulation whereas the experimental spectroscopy is done with material in a significant amount

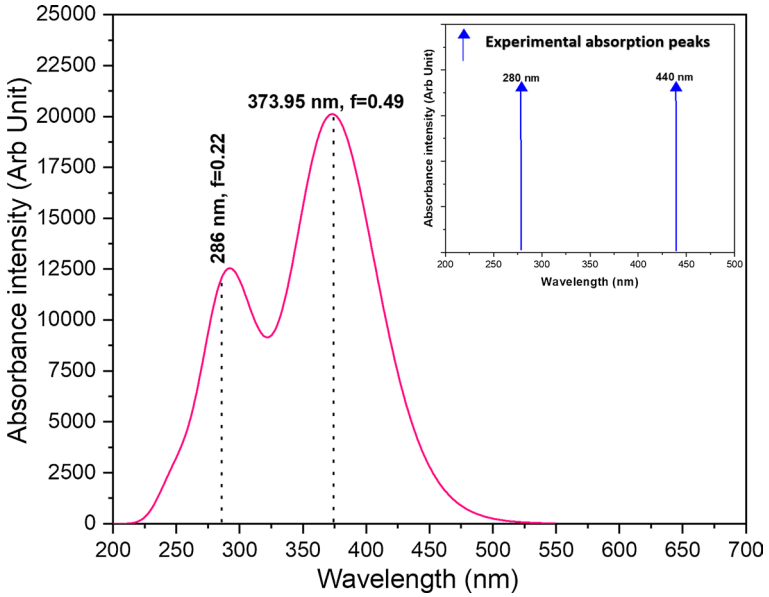

Fig. 6 Simulated absorption spectra of DNP molecule showing highest transition peaks of two bands between 200–325 and 330–475 nm. Inset of the Fig. 6 shows the highest transition peaks obtained between bands 250–310 and 350–460 nm of the experimental absorption spectra drawn in accordance with the experimental details given in (Brister et al. 2017)

with multiple molecules. The range of absorption spectra indicate the existence of π- π* and n- π* transitions. The occurrence of π- π* and n- π* transitions are validated by the experimental references also and enhance the possibility of intramolecular interactions (Rana et al. 2017). Generally, π–π* transition are responsible for the formation of strong absorption peak between 300–500 nm wavelength and n–π* transition gives absorption peak below 500 nm. Thus, both the computational and experimental range of the absorption peaks reflects the π- π* and n- π* like nature of electronic transitions of the DNP molecule. The lowest excitation energy for DNP was 3.31 eV which was approximately same as the HOMO-LUMO gap i.e., 3.16 eV. The difference between the excitation energy and band gap might be due to the basis functions that are used for the calculation of excitation energy and band gap. The DFT calculation is done for the ground state geometry with the given set of functions. Band gap computed using the Koopman's equations have functions orthogonal. Whereas, the TD-DFT calculation is done for excited state and the best linear combination of the given functions are preferred for the excited state calculations. In excited state functions are not orthogonal and thus give lower energy as the excitation energy (Hutter and Hutter 2003). The UV-Vis spectral analysis reveals transition arising out of the interaction between the lone pair (n) electrons and the π electrons. These transitions were responsible for the higher NLO activity of DNP.

3.7 Nuclear magnetic resonance (NMR) analysis

NMR analysis was performed for DNP and nuclear spin was used for performing structural analysis (Fleck et al. 2010). All the chemical shifts are listed in SD 6 and the chemical shifts of H atoms and C atoms are shown in SD 7. Tetramethylsilane (TMS) at 298.15 K temperature and 1 bar pressure is considered the internal reference compound. The 12 carbon atoms of the TMS structure lead to a sharp resonance line preventing the interference of the 1H structures with the other resonating structures. This makes TMS an established internal reference compound (Rana et al. 2018). As the nitro groups and C–H bonds of the benzene ring are the most chemically reactive parts of the DNP, the higher chemical shifts are observed for atoms associated with these bonds. All the aromatic carbon atoms bonded with 17C–25H, 20C–28H, 22C–30H, 21C–29H, and 18C–26H bonds have chemical shifts 144.7, 139.49, 134.6, 139.47, and 144.7 ppm respectively. The experimental NMR spectra of DNP molecule is also available in PubChem. For better validation of the result the computed 13C NMR spectra was compared with the experimental data available in PubChem. The experimental NMR shifts for 13C available in PubChem has chemical shift around 142 ppm which is quite close to these values and the slight variation might be due to the experimental values are corresponding to material and simulated spectra deals with the single molecule (https://pubchem.ncbi.nlm.nih.gov/compound/1_3-dinitropyrene#section=Spectral-Information). These shifts are larger than the carbon atoms attached to the C–H bonds. The high chemical shifts observed for carbon atoms of C–H bonds are mainly due to the availability of the hydrogen bond between the C–H bond. Availability of the hydrogen bonding leads to the de-shielding of the protons giving rise to the chemical peaks. Higher values of the chemical shifts are obtained for oxygen atoms 1O (602.24 ppm), 2O (602.24 ppm), 3O (624.6 ppm), and 4O (624.6 ppm). These higher values are due to the resonating effect of the nitro group that makes it highly electron-withdrawing. Thus, the higher value of chemical shifts in hydrogen and oxygen atoms shows that the molecule exhibits strong ICT. Hence, it can be said that the high chemical shifts lead to the high polarizability of the DNP molecule enhancing its candidature as an NLO active molecule.

3.8 Nonlinear optical analysis

The behavior of the materials when kept in external electric field is accounted by the polarization. The NLO activity of any molecule can be predicted by the polarizability parameters. When molecules with multiple atoms are put on in such field, a large cluster of charge cloud is emerged from the molecule that leads to the ICT. This charge transfer leads to the high value of polarizability. Thus, for investigating the NLO activity of the DNP, polarizability parameters like μ_{total}, α_{total} and β_{total} are computed (all the tensor components of the NLO parameters are mentioned in SD 8). For DNP, the computed values of μ_{total},α_{total} and $\Delta\alpha$ are 3.39 Debye, 33.16×10^{-24} esu and 99.44×10^{-24} esu respectively. The value of μ_{total} is found two times higher than that of generally used reference organic NLO material Urea (1.52 Debye). The value of α_{total} of the DNP is five times higher than α_{total} of Urea (5.66×10^{-24} esu). The value of $\Delta\alpha$ of the DNP is fifteen times higher than that of Urea (6.30×10^{-24} esu). These values show the enhanced optical behavior of DNP molecule. The electronic transitions between the donor and acceptor moieties introduces immense ICT in the probe molecule. For investigating the optical non

linearity, coefficients of the higher order terms of the Taylor's series expansion (say β_{total}) is computed using finite field theory approach. Extreme high value of β_{total} is obtained for the DNP. The β_{total} is computed as 21.02×10^{-30} esu. For the validation of the computed results, the β_{total} of the DNP is compared with the β_{total} of fifteen materials that are experimentally proven NLO active. SD 9 lists the reference materials that were used for the comparison. The β_{total} of the DNP was found nearly twenty seven times higher than Urea (0.78×10^{-30} esu), ten times higher than phenyl urea and five times higher than thiourea glutaric acid. When compared with other reference materials, β_{total} of the DNP was three times higher than L-Leucine nitrate, fifteen times higher than 3-nitroaniline, six times higher than Creatinium L-tartarate monohydrate, and one and half times higher than 2-methyl 4-nitro aniline and 9-anthraldehyde. Three thiosemicarbazone derivatives mentioned in SD 9 are also used for the comparison. The β_{total} of the DNP is found nine times higher than benzyl derivative of thiosemicarbazone, sixteen times higher than chlorobenzyl derivative of thiosemicarbazone and six times higher than bromobenzyl derivative of thiosemicarbazone. The DNP has β_{total} 1.7 times higher than β_{total} of Trans-4-hydroxyl-1-proline (12.23×10^{-30} esu). Indole-7-carboxaldehyde (3.96×10^{-30} esu) and ANDIROBIN (methyl-2{(1R,2R)-2- [(1aS, 4S, 4aS, 8aS)-4-(furan-3-yl)-4a-methyl-8-methylene2-oxooctahydrooxireno[2,3-d] isochromen-7-yl]-2,6,6- trimethyl-5-oxocyclohex-3-en-1-yl} acetate) (3.75×10^{-30}) have β_{total} nearly close to each other. Thus, the β_{total} of the DNP is five times higher than these two molecules. The DNP has β_{total} nearly four times higher than 2,4,6-triaminopyramidine. The comparison of the β_{total} of the title molecules with reference molecules is graphically illustrated in Fig. 7. This comparison fairly suggest that the DNP is a highly chemically reactive molecule with potent NLO activities. Thus, the presented computational study suggests that the DNP molecule can be a better NLO responsive material and can be used as various NLO applications in future.

3.9 OLED and LHE analysis

The preliminary calculation of the RE is used to develop the candidature of the DNP molecule for the application of OLED devices. The smaller magnitude of the RE provides general insight into the easy charge transportability of the DNP (Gao and Gao 2010). The hole RE and electron RE for the DNP molecule is computed as 0.3204 and 0.3211 eV respectively. The reduced value of hole RE as compared to electron RE shows that DNP has better hole transportability. However, the insignificant difference shows the ability of DNP to be used as both electron transfer material and hole transfer material. Materials having the ability to transfer holes as well as electrons are termed ambipolar materials (Sun et al. 2017). Thus, it can be said that DNP can be also used as ambipolar charge-transfer material. Although, the materials having high electron RE values can be used in electron blocking applications. The hole RE for title molecule is comparable to the hole RE of typical hole transferring materials, N, N'-diphenyl-N, N'-bis(3-methyl phenyl) -(1,1'-biphenyl)-4,4'-diamine (0.290 eV) and 4,4' - bis(1-naphthylphenylamino) biphenyl (0.295 eV) (Malagoli et al. 2000; Tong et al. 2007). These nonlinear acenes show better hole transportability. These results suggest that DNP can be used as a hole transport layer in OLEDs. The LHE of the DNP molecule is computed using f (0.3997) obtained for the $S_0 \rightarrow S_1$ transition of absorption spectra. The value of 60.09 is obtained for DNP. This implies that the DNP molecule can convert 60% light energy into electrical energy and this can be used along with other dyes which are presently used as photosensitizers in DSSCs.

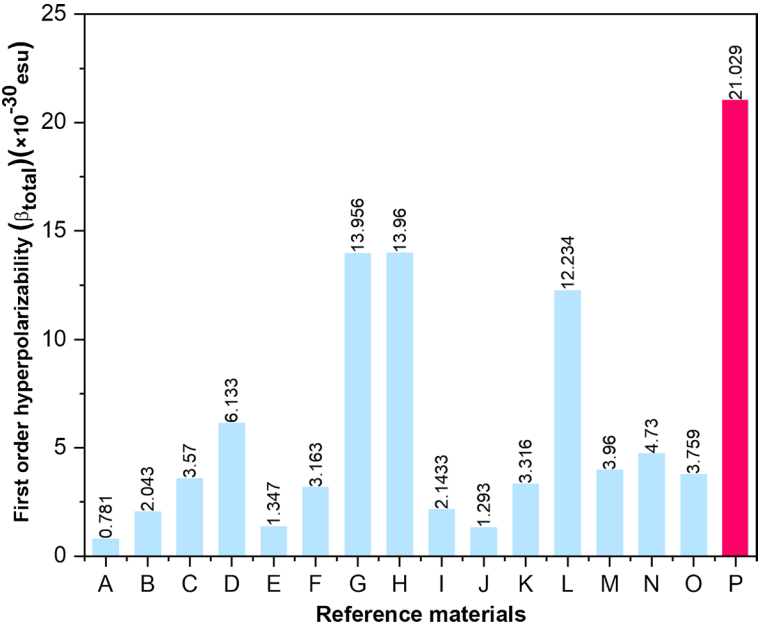

Fig. 7 Graph showing comparison between the β_{total} of the reference materials and DNP. The alphabets represents the reference compound: **A**=urea (Cassidy et al. 1979),**B**=phenyl urea (Marappan et al. 2019),**C**= thiourea-glutaric acid (Thirumurugan et al. 2018),**D**= L-Leucine nitrate (Vennila et al. 2018),**E**=3-nitroaniline (Krishnakumar et al. 2008),**F**=Creatinium L-tartarate monohydrate (Thirumurugan et al. 2017),**G**=2-methyl 4-nitro aniline (Shankar et al. 2021),**H**=9-anthraldehyde (Vijayalakshmi et al. 2014),**I**=(E/Z)-4-(4-chlorobenzyl)-1-(1-ferrocenyl-ethyl) thiosemicarbazone (Jawaria et al. 2019),**J**=(E/Z)-4-(4-chlorobenzyl)-1-(1-ferrocenyl-ethyl) thiosemicarbazone (Jawaria et al. 2019),**K**=(E/Z)-4-(2-bromo benzyl)-1-(1-ferrocenylethyl) thiosemicarbazone (Jawaria et al. 2019),**L**=trans-4-hydroxy-l-proline (Thirumurugan et al. 2017),**M**=Indole-7-carboxaldehyde (Rana et al. 2020),**N**=2,4,6-triaminopyramidine (Faizan et al. 2021),**O**=ANDIROBIN (Abe et al. 2021), and **P**=DNP.

4 Conclusion

The computational results in the current study established that like other pyrene derivatives, the DNP has high chemical reactivity. The reactivity mainly arises due to the availability of donating C–H bonds of the benzene rings and two nitro groups that acts as electron-withdrawing agents. ICT was observed and verified between these two groups with the help of Mulliken charge distribution and MEP surface. The vibrational modes with high Raman intensity are observed for the bonds corresponding to C–H and nitro groups. Thus, the theoretical calculations performed for DNP reveal that the molecule possesses excellent first-order NLO responses. These responses arise due to the π- conjugated donor and acceptor parts. In comparison to the typical hole transport material, there seems a reduction in the hole RE, suggesting the utility of DNP towards the OLED devices. Thus, the theoretical study concludes the high NLO activity of the DNP molecule and it can be said that the experimental verifications performed with this molecule will not be disappointing. Also, it is believed that the current study will provide the benchmark data of reference NLO materials at different levels for the theoretical community and will give insights to the experimental community to design better NLO materials for hi-tech NLO applications.

Supplementary Information The online version contains supplementary material available at https://doi.org/10.1007/s11082-022-04371-7.

Authors' contributions Shradha Lakhera: Data curation, Writing-Original draft preparation, Visualization,Investigation, Software, Validation. Meenakshi Rana: Conceptualization, Methodology, Writing-Reviewing and Editing, Supervision Kamal Devlal: Conceptualization, Writing- Reviewing and Editing Vivek Dhuliya: Visualization, Investigation, Software, Validation.

Funding The authors declare that this research received no specific grant from any funding agency.

Data Availability All data generated or analysed during this study, which support the plots within this paper and the other findings of this study, are included in this article and its Supplementary Information. Source data are provided with this paper.

Declarations

Conflict of interests The authors declare that they have no known competing financial interests or personal relationships that could have appeared to influence the work reported in this paper.

Ethical approval This material is the authors' own original work, which has not been previously published elsewhere. All authors have been personally and actively involved in substantial work leading to the paper, and will take public responsibility for its content. The paper properly credits the meaningful contributions of all the co-authors.

References

Abe, M.T.O., Nzia, C.L., Sidjui, L.S., Kamsi, R.A.Y., Mveme, C.D.D., Assatse, Y.T., Ndjaka, J.M.B., Ejuh, G.W.: Predictive calculation of structural, nonlinear optical, electronic and thermodynamic properties of andirobin molecule from ab initio and DFT methods. SN Appl. Sci. **3**, 768 (2021). https://doi.org/10.1007/s42452-021-04749-4

Abusaif, M.S., Fathy, M., Abu-Saied, M.A., Elhenawy, A.A., Kashyout, A.B., Selim, M.R., Ammar, Y.A.: New carbazole-based organic dyes with different acceptors for dye-sensitized solar cells: Synthesis, characterization, dssc fabrications and density functional theory studies. J. Mol. Struct. **1225**, 129297 (2021). https://doi.org/10.1016/j.molstruc.2020.129297

Abusaif, M.S., Fathy, M., Abu-Saied, M.A., Elhenawy, A.A., Kashyout, A.B., Selim, M.R., Ammar, Y.A.: New carbazole-based organic dyes with different acceptors for dye-sensitized solar cells: Synthesis, characterization, dssc fabrications and density functional theory studies. J. Mol. Struct. **1225**, 129297 (2021). https://doi.org/10.1016/j.molstruc.2020.129297

Abusaif, M.S., Fathy, M., Abu-Saied, M.A., Elhenawy, A.A., Kashyout, A.B., Selim, M.R., Ammar, Y.A.: New carbazole-based organic dyes with different acceptors for dye-sensitized solar cells: Synthesis, characterization, dssc fabrications and density functional theory studies. J. Mol. Struct. **1225**, 129297 (2021). https://doi.org/10.1016/j.molstruc.2020.129297

Andijani, N., Al-Qurashi, O., Wazzan, N., Irfan, A.: Modeling of efficient pyrene-core substituted with electron-donating groups as hole-transporting materials in perovskite solar cells. Sol Energy. **188**, 898–912 (2019). https://doi.org/10.1016/j.solener.2019.06.074

Andijani, N., Wazzan, N.A.: The effect of electron-donating substituents on tuning the nonlinear optical properties of pyrene-core arylamine derivatives: DFT calculations. Results Phys. **11**, 605–616 (2018). https://doi.org/10.1016/j.rinp.2018.10.002

Becke, A.D.: Density-functional thermochemistry. III. The role of exact exchange. J. Chem. Phys. **98**(7), 5648–5652 (1993). https://doi.org/10.1063/1.464913

Becke, A.D.: Density-functional thermochemistry. V. Systematic optimization of exchange-correlation functionals. J. Chem. Phys. **107**, 8554–8560 (1997). https://doi.org/10.1063/1.475007

Bhatt, H., Pant, T., Dhoundiyal, C.C., Rana, M., Chowdhury, P., Joshi, G.C., Arya, P., Tiwari, H.: Computational study of the intermolecular interactions and their effect on the UV-visible spectra of the ternary liquid mixture of benzene, ethanol and propylene glycol. J. Mol. Model. **26**, 268 (2020). https://doi.org/10.1007/s00894-020-04533-y

Brister, M.M., Santiago, L.E.P., Morel, M., Arce, R., Crespo-Hernández, C.E.: Photochemical relaxation pathways in dinitropyrene isomer pollutants. J. Phys. Chem. A. (2017). https://doi.org/10.1021/acs.jpca.7b04769

Buriahi, A., Singh, M.S., Arslan, V.P.: Gamma-ray attenuation properties of some NLO materials: potential use in dosimetry. Radiat Environ Biophys. **59**, 145–150 (2020). https://doi.org/10.1007/s00411-019-00824-y

Cassidy, C., Halbout, J.M., Donaldson, W., Tang, C.L.: Nonlinear optical properties of urea. Opt. Commun. **29**(2), 243–246 (1979). https://doi.org/10.1016/0030-4018(79)90027-0

Chen, Q., Siddique, F., Silva, G.T.M., Lischka, H., Quina, F.H., Aquino, A.J.A.: Ab initio calculation of the excited states of nitropyrenes. Theor. Chem. Acc. **140**, 97 (2021). https://doi.org/10.1007/s00214-021-02791-4

Curutchet, C., Mennucci, B.: Quantum chemical studies of light harvesting. Chemical Reviews. **117**(2), 294–343 (2017). https://doi.org/10.1021/acs.chemrev.5b00700

Dennington R., Keith T., Millam J.: GaussView, Version 4.1.2, Semichem, Inc., Shawnee Mission, KS (2007)

Faizan, M., Mehkoom, M., Afroz, Z., Rodrigues, V.H.N., Afzal, S.M., Ahmad, S.: Experimental and computational investigation of novel dihydrated organic single crystal of 2,4,6-triaminopyrimidine and 3,5-dintrobenzoic acid: Linear and nonlinear optical response with limiting performance. J. Solid State Chem. **300**, 122255 (2021). https://doi.org/10.1016/j.jssc.2021.122255

Felscia, U.R., Rajkumar, B.J.M., Mary, M.B.: Charge transport properties of pyrene and its derivatives: optoelectronic and nonlinear optical applications. J. Mater. Sci. **53**, 15213–15225 (2018). https://doi.org/10.1007/s10853-018-2690-9

Felscia, U.R., Rajkumar, B.J.M., Mary, M.B.: Theoretical investigations on nonlinear fused 4-ring systems: Application to OLED and NLO devices. Synth. Met. **246**, 31–38 (2018). https://doi.org/10.1016/j.synthmet.2018.09.008

Fleck, M., Petrosyan, A.M.: Difficulties in the growth and characterization of non-linear optical materials: a case study of salts of amino acids. J. Cryst. Growth. **312**(15), 2284–2290 (2010). https://doi.org/10.1016/j.jcrysgro.2010.04.054

Frisch M.J., Trucks G.W., Schlegel et al. H.B.: Gaussian 09, Revision B. 01, Gaussian Inc., Wallingford CT. 121: 150-166, (2009)

Gao, H.: Theoretical investigation into charge mobility in 4,4′-bis(1-naphthylphenylamino)biphenyl. Theor. Chem. Acc. **127**, 759–763 (2010). https://doi.org/10.1007/s00214-010-0804-9

Hutter, J.: Excited state nuclear forces from the Tamm-Dancoff approximation to time-dependent density functional theory within the plane wave basis set framework. J. Chem. Phys. **118**(9), 3928–3934 (2003). https://doi.org/10.1063/1.1540109

Jawaria, R., Hussain, M., Khalid, M., Khan, M.U., Tahir, M.N., Naseer, M.M., Braga, A.A.C., Shafiq, Z.: Synthesis, crystal structure analysis, spectral characterization and nonlinear optical exploration of potent thiosemicarbazones based compounds: a DFT refine experimental study. Inorg. Chim. Acta. **486**, 162–171 (2019). https://doi.org/10.1016/j.ica.2018.10.035

Jeyaram, S., Geethakrishnan, T.: Spectral and third-order nonlinear optical characteristics of natural pigment extracted from coriandrum sativum. Opt. Mater. **107**, 110148 (2020). https://doi.org/10.1016/j.optmat.2020.110148

John, N.L., Abraham, S., Sajan, D., Philip, R., Joy, N., Chitra, R.: Molecular structure, NLO properties and vibrational analysis of l-Histidine tetra fluro borate by experimental and computational spectroscopic techniques. Spectrochim. Acta A Mol. Biomol. Spectrosc. **226**, 117615 (2020). https://doi.org/10.1016/j.saa.2019.117615

Khalid, M., Lodhi, H.M., Khan, M.U., Imran, M.: Structural parameter-modulated nonlinear optical amplitude of acceptor–π–D–π–donor-configured pyrene derivatives: a DFT approach. RSC Adv. **11**, 14237–14250 (2021)

Koopmans, T.: Ordering of wave functions and eigenenergies to the individual electrons of an atom. Physica. **1**, 104–113 (1933). https://doi.org/10.1016/S0031-8914(34)90011-2

Krishnakumar, V., Nagalakshmi, R.: Studies on the first-order hyperpolarizability and terahertz generation in 3-nitroaniline. Phys. B: Condens. Matter. **403**(10–11), 1863–1869 (2008). https://doi.org/10.1016/j.physb.2007.10.341

Lakhera, S., Devlal, K., Ghosh, A., Rana, M.: In silico investigation of phytoconstituents of medicinal herb 'Piper Longum' against SARS-CoV-2 by molecular docking and molecular dynamics analysis. Results Chemistry. **3**, 100199 (2021). https://doi.org/10.1016/j.rechem.2021.100199

Lakhera, S., Devlal, K., Ghosh, A., Rana, M.: Modelling the DFT structural and reactivity study of feverfew and evaluation of its potential antiviral activity against COVID-19 using molecular docking and MD simulations. Chem. Pap. **76**, 2759–2776 (2022). https://doi.org/10.1007/s11696-022-02067-6

Lakhera, S., Devlal, K., Rana, M., Celik, I.: Study of nonlinear optical responses of phytochemicals of Clitoria ternatea by quantum mechanical approach and investigation of their anti-Alzheimer activity with in silico approach. Struct Chem (2022). https://doi.org/10.1007/s11224-022-01981-5

Lakhera, S., Devlal, K., Rana, M., Dhuliya, V.: Quantum mechanical study of three aromatic bioactive fatty alcohol compounds with nonlinear optical and potential light harvesting properties. Opt. Mater. **129**, 112476 (2022). https://doi.org/10.1016/j.optmat.2022.112476

Lakhera, S., Rana, M., Devlal, K., Celik, I., Yadav, R.: A comprehensive exploration of pharmacological properties, bioactivities and inhibitory potentiality of luteolin from Tridax procumbens as anticancer drug by in-silico approach. Struct. Chem. (2022). https://doi.org/10.1007/s11224-022-01882-7

Malagoli, M., Brédas, J.L.: Density functional theory study of the geometric structure and energetics of triphenylamine-based hole-transporting molecules. Chem. Phys. Lett. **327**(1–2), 13–17 (2000). https://doi.org/10.1016/S0009-2614(00)00757-0

Marappan, D., Palanisamy, M., Shu, M., Balraj, B., Sivakumar, C.: Growth, vibrational, optical, mechanical and DFT investigations of an organic nonlinear optical material – Phenylurea. Zeitschrift für Physikalische Chemie. **233**(11), 1659–1682 (2019). https://doi.org/10.1515/zpch-2018-1230

Mary, Y.S., Bolelli, T.E., Thomas, R., Krishnan, A.R., Bolelli, K., Kasap, E.N., Onkol, T., Yildiz, I.: Quantum mechanical studies of three aromatic halogen-substituted bioactive sulfonamidobenzoxazole compounds with potential light harvesting properties. Polycycl Aromat Compd. (2019). https://doi.org/10.1080/10406638.2019.1689405

More, A.B., Sekar, N.: Nonlinear optical properties of pyrene based fluorescent hemicurcuminoid and their BF_2 complexes –spectroscopic and DFT studies. J. Fluoresc. **27**, 1777–1792 (2017). https://doi.org/10.1007/s10895-017-2116-0

Nagarajan, B., Kushwaha, S., Elumalai, R., Mandal, S., Ramanujam, K., Raghavachari, D.: Novel ethynyl-pyrene substituted phenothiazine based metal free organic dyes in DSSC with 12% conversion efficiency. J. Mater. Chem. A **5**, 10289–10300 (2017). https://doi.org/10.1039/C7TA01744H

Niu, R., Chang, Q., Wu, X., Han, Y., Jia, J., Chen, S., Song, Y.: D-π-A type conjugated pyrene derivatives: Third-order nonlinear absorption and excited-state dynamics. Opt. Mater. **85**, 319–328 (2018). https://doi.org/10.1016/j.optmat.2018.08.073

Nuclear magnetic resonance (NMR) spectra of 1,3-ditropyrene, PubChem. https://pubchem.ncbi.nlm.nih.gov/compound/1_3-dinitropyrene#section=Spectral-Information

Ojo, N.D., Krause, R.W., Egbedi, N.O.O.: Electronic and nonlinear optical properties of 3-(((2-substituted-4-nitrophenyl)imino)methyl)phenol. Comput. Theor. Chem. **1192**, 113050 (2020). https://doi.org/10.1016/j.comptc.2020.113050

Ozarslan, A., Çakmaz, D., Erol, F., Şenöz, H., Seferoğlu, N., Barsella, A., Seferoğlu, Z.: Synthesis and investigation of photophysical, NLO and thermal properties of D-π-A-π-D dyes. J. Mol. Struct. (2020). https://doi.org/10.1016/j.molstruc.2020.129583

Rana, M., Chatterjee, A., Chowdhury, P.: Investigation of nonlinear optical properties of organic based di amine substituted tetraphenylethylene. AIP Conf. Proc. **2009**, 020055 (2018). https://doi.org/10.1063/1.5052124

Rana, M., Chowdhury, P.: Nonlinear optical responses of organic based indole derivative: an experimental and computational study. Mater. Today: Proc. **28**(1), 241–245 (2020). https://doi.org/10.1016/j.matpr.2020.01.598

Rana, M., Singla, N., Chatterjee, A., Shukla, A., Chowdhury, P.: Investigation of nonlinear optical (NLO) properties by charge transfer contributions of amine functionalized tetraphenylethylene. Opt. Mater. **62**, 80–89 (2016). https://doi.org/10.1016/j.optmat.2016.09.043

Rana, M., Singla, N., Pathak, A., Dhanya, R., Narayana, C., Chowdhury, P.: Vibrational & electronic properties of intra/inter molecular hydrogen bonded heterocyclic dimer: an experimental and theoretical study of pyrrole-2-carboxaldehyde. Vib. Spectrosc. **89**, 16–25 (2017). https://doi.org/10.1016/j.vibspec.2016.12.003

Rana, M., Singla, N., Pathak, A., Dhanya, R., Narayana, C., Chowdhury, P.: Vibrational-electronic properties of intra/inter molecular hydrogen bonded heterocyclic dimer: an experimental and theoretical study of pyrrole-2-carboxaldehyde. Vib. Spectrosc. **89**, 16–25 (2017). https://doi.org/10.1016/j.vibspec.2016.12.003

Ray, P.C.: Size and shape dependent second order nonlinear optical properties of Nanomaterials and their applications in biological and chemical sensing. Chem. Rev. **110**(9), 5332–5365 (2010). https://doi.org/10.1021/cr900335q

Sang-aroon, W., Tontapha, S., Amornkitbamrung, V.: Photovoltaic performance of natural dyes for dye-sensitized solar cells: a combined experimental and theoretical study. Dye-Sensitized Solar Cells. (2019). https://doi.org/10.1016/B978-0-12-814541-8.00006-9

Sethi, A., Prakash, R.: Novel synthetic ester of Brassicasterol, DFT investigation including NBO, NLO response, reactivity descriptor and its intramolecular interactions analyzed by AIM theory. J. Mol. Struct. **1083**, 72–81 (2015). https://doi.org/10.1016/j.molstruc.2014.11.028

Shankar, M., Thirupugalmani, K., Nehru, K., Athimoolam, S., Tamilmani, V., Potheher, I.V.: 2-Methyl-4-Nitroaniline derived novel organic NLO crystal: experimental and theoretical analysis. J. Mol. Struct. **1243**, 130905 (2021). https://doi.org/10.1016/j.molstruc.2021.130905

Shi, Y., Li, Z., Fang, Y., Sun, J., Zhao, M., Song, Y.: Ultrafast third-order nonlinear optical response of pyrene derivatives. Opt. Laser Technol. **90**, 18–21 (2017). https://doi.org/10.1016/j.optlastec.2016.11.003

Si, Y., Yang, G.: Theoretical study on the second-order nonlinear optical properties and reorganization energy of silafluorenes and spirobisilafluorenes derivatives. Theor Chem Acc. **128**, 249–256 (2011). https://doi.org/10.1007/s00214-010-0838-z

Sun, F., Jin, R.: DFT and TD-DFT study on the optical and electronic properties of derivatives of 1,4-bis(2-substituted-1,3,4-oxadiazole)benzene. Arab. J. Chem. **10**(2), S2988–S2993 (2017). https://doi.org/10.1016/j.arabjc.2013.11.037

Sun, J., Wang, G., Liu, C., Shi, Y., Zhao, M.: Synthesis of four pyrene-containing chalcone derivatives: achieving excellent third-order nonlinear optical properties by optimizing halopyridines. Opt. Laser Technol. **109**, 600–607 (2019). https://doi.org/10.1016/j.optlastec.2018.08.038

Tang, F., Wu, K., Zhou, Z., Wang, G., Zhao, B., Tan, S.: Alkynyl-functionalized Pyrene-cored Perylene diimide electron acceptors for efficient nonfullerene organic solar cells. ACS Appl. Energy Mater. **2**(5), 3918–3926 (2019). https://doi.org/10.1021/acsaem.9b00611

Thirumurugan, R., Anitha, K.: Growth, structural, physical and computational perspectives of trans-4-hydroxy-l-proline: a promising organic nonlinear optical material with large laser-induced damage threshold. Mater. Res. Express. **4**(5), 056202 (2017). https://doi.org/10.1088/2053-1591/aa6072

Thirumurugan, R., Babu, B., Anitha, K., Chandrasekaran, J.: Experimental and density functional theory (DFT): a dual approach to probe the key properties of creatininium L-tartrate monohydrate single crystal for nonlinear optical applications. J. Mol. Struct. (2017). https://doi.org/10.1016/j.molstruc.2017.07.095

Thirumurugan, R., Babu, B., Anitha, K., Chandrasekaran, J.: Synthesis, growth, characterization and quantum chemical investigations of a promising organic nonlinear optical material: thiourea-glutaric acid. J. Mol. Struct. **1171**, 915–925 (2018). https://doi.org/10.1016/j.molstruc.2017.07.027

Tong, Q.X., Lai, S.L., Chan, M.Y., Lai, K.H., Tang, J.X., Kwong, H.L., Lee, C.S., Lee, S.T.: High Tg Triphenylamine-based starburst hole-transporting material for organic light-emitting devices. Chem. Mater. **19**(24), 5851–5855 (2007). https://doi.org/10.1021/cm0712624

Vennila, P., Govindaraju, M., Venkatesh, G., Kamal, C., Mary, Y.S., Panicker, C.Y., Kaya, S., Armaković, S., Armaković, S.J.: A complete computational and spectroscopic study of 2-bromo-1, 4-dichlorobenzene – A frequently used benzene derivative. J. Mol. Struct. **1151**, 245–255 (2018). https://doi.org/10.1016/j.molstruc.2017.09.049

Vijayalakshmi, S., Kalyanaraman, S.: DFT and TD-DFT approach for the analysis of NLO and OLED applications of 9-anthraldehyde. Optik. **125**(10), 2429–2432 (2014). https://doi.org/10.1016/j.ijleo.2013.10.104

Wazzan, N., El-Shishtawy, R.M., Irfan, A.: DFT and TD–DFT calculations of the electronic structures and photophysical properties of newly designed pyrene-core arylamine derivatives as hole-transporting materials for perovskite solar cells. Theor. Chem. Acc. (2018). https://doi.org/10.1007/s00214-017-2183-y

Yadav, P., Rana, M., Chowdhury, P.: DFT and MD simulation investigation of favipiravir as an emerging antiviral option against viral protease (3CLpro) of SARS-CoV-2. J. Mol. Struct. **1246**, 131253 (2021). https://doi.org/10.1016/j.molstruc.2021.131253